REDIN Revista Facultad de Ingeniería Universidad de Antioquia

No.117, pp. 9-21, Oct-Dec 2025

Chromium adsorption using a composite adsorbent of corn waste and bentonite

Adsorción de cromo con un adsorbente compuesto de residuos de maíz y bentonita

Miguel Eduardo Herrera-Gavidia [1], Dalia Carbonel [1*], Hugo Chirinos-Collantes [1]

[1]Facultad de Ingeniería Ambiental, Universidad Nacional de Ingeniería. 210 Tupac Amaru Avenida 15333. Lima, Peru.

CITE THIS ARTICLE AS:

M. E. Herrera-Gavidia, D. Carbonel and H. Chirinos-Collantes. "Chromium adsorption using a composite adsorbent of corn waste and bentonite", *Revista Facultad de Ingeniería Universidad de Antioquia*, no. 117, pp. 9-21, Oct-Dec 2025. [Online]. Available: https://www.doi.org/10.17533/udea.redin.20241249

ARTICLE INFO:

Received: December 12, 2023
Accepted: December 02, 2024
Available online: December 04, 2024

KEYWORDS:

Clay; metals; organic matter; statistics

Arcilla; estadística; metales; materia orgánica

ABSTRACT: Chromium, a highly toxic heavy metal, poses significant risks to both human health and environmental quality. Its adsorption in wastewater using low-cost, easily implementable technologies has emerged as a crucial solution for mitigating its harmful impact. This study explores the effectiveness of a composite adsorbent made from bentonite and corn waste for chromium adsorption. Experiments were conducted in a laboratory-scale batch system. The research examined the adsorption kinetics and equilibrium, process optimization, and the mechanisms of chromium adsorption. For optimization, a response surface methodology was applied considering three variables: adsorption time (min), adsorbent dosage (g/L), and initial chromium concentration (mg/L). The findings suggest that the adsorption kinetics fit best with the pseudo-first-order model (R^2 = 0.968), and the adsorption equilibrium fits with the Freundlich model (R^2 = 0.997). During optimization, the adsorbent dosage emerged as the most critical factor for chromium removal. The optimal operating conditions were determined to be 103 minutes, 29.71 g/L of adsorbent, and an initial chromium concentration of 31.13 mg/L. The results indicate that chromium adsorption is a multifaceted process involving diffusion and subsequent interaction at the surface and edges of the bentonite layers. Chemical analysis, coupled with changes in the FTIR spectrum, suggests an interaction between chromium and the silicon and aluminum components of the bentonite. These findings underscore the potential of the composite adsorbent for effective chromium removal.

RESUMEN: El cromo es un metal pesado que representa un riesgo para la salud humana y la calidad ambiental. Su adsorción de aguas residuales, con tecnologías sencillas y económicas, se ha convertido en una solución clave para mitigar su impacto. En este estudio se exploró la eficacia de un adsorbente compuesto de bentonita y residuos de maíz en la adsorción del cromo. La investigación analizó la cinética y el equilibrio de adsorción, la optimización del proceso y los mecanismos de adsorción. Para la optimización se empleó un diseño de superficie de respuesta considerando: tiempo de adsorción (min), dosis de adsorbente (g/L) y concentración inicial de cromo en solución (mg/L). Los resultados indican que la cinética de adsorción se ajusta al modelo de pseudo-primer orden (R^2 = 0.968) y el equilibrio de adsorción se ajusta al modelo de Freundlich (R^2 = 0.997). En la optimización, la dosis del adsorbente fue el factor más crítico. Las condiciones óptimas de operación son: 103 minutos, 29.71 g/L de adsorbente y 31.13 mg/L de concentración inicial de cromo. Los resultados sugieren que la adsorción del cromo es un proceso multifacético que implica difusión y una interacción posterior en la superficie y en los bordes de las capas de la bentonita. El análisis químico, junto con los cambios en el espectro FTIR, apuntan a una interacción entre el cromo con el silicio y aluminio de la bentonita.

1. Introduction

Chromium, recognized both as a transition and heavy metal, is omnipresent in the environment. Due to its toxic characteristics and properties, exposure

* Corresponding author: Dalia Carbonel
E-mail: dcarbonelr@uni.pe
ISSN 0120-6230
e-ISSN 2422-2844

significantly heightens human health risks and degrades environmental quality [1]. A particularly hazardous aspect of chromium is its toxicity at minimal concentrations coupled with a worsening cumulative impact [2].

Industrial sources are predominantly responsible for chromium emissions in the environment, specifically from sectors like chemical processing and manufacturing, mineral handling, steel production, metal finishing, leather tanning, textile dyeing, electroplating, cement production, metallurgy, and other related fields [3, 4]. Chromium, utilized in these industrial processes, also features prominently in their effluents and wastes. The release of untreated wastewater marks a critical pathway for environmental chromium contamination [5]. Once in aquatic systems, the hazard of chromium lies in its mobility and ease of integration into the food chain [1]. Thus, devising an effective method for its removal prior to environmental discharge is crucial.

In Peru, the contamination of wastewater with chromium has emerged as a significant environmental and public health concern. Following the conventional tannery process, the chromium concentration of wastewater can reach 500 mg/L [6]. In Peru, the maximum permissible concentration of chromium in non-domestic wastewater discharged into the sanitary sewer system is 10 mg/L of total chromium and 0.5 mg/L of chromium VI. Consequently, companies are obliged to treat the effluent prior to its discharge. [7] estimate that between 20 and 40% of the total chromium used by tanneries in cities such as Lima, Arequipa, and Trujillo is discharged without prior treatment. A comparable situation is observed in Arequipa at the Río Seco Industrial Park in Cerro Colorado [8].

Elimination of chromium from effluents in wastewater treatment facilities can be accomplished via primary methods such as precipitation or chemical reduction [9], secondary methods like bioremediation, or tertiary methods including ion exchange or adsorption [10]. While primary treatments are effective, they generate substantial volumes of hazardous waste [9]. Bioremediation, although advantageous, might face setbacks due to microorganism inhibition at high metal concentrations [10]. Conversely, cation exchange, in spite of its effectiveness, is limited by its technological and operational demands, requiring sophisticated machinery and skilled operators [10].

Alternatively, adsorption of heavy metals offers a straightforward, cost-effective solution that minimizes waste generation. The technique of chromium adsorption from wastewater has gained considerable attention as a feasible treatment option owing to its affordability and operational simplicity [11]. Promising and economical adsorbents include those derived from biomass and clay [12], both readily available and thus cost-effective.

Clays have been exhaustively researched for heavy metal adsorption [10], including chromium in aqueous environments [13]. Research in this area has shown that materials such as bentonite can be effective in extracting Cr (III) and Ni (II) from industrial wastewater, with recorded maximum adsorption capacities of 90.91 mg/g for chromium and 9.94 mg/g for nickel, respectively [14].

Utilizing biomass-based adsorbents offers the potential for repurposing organic wastes, a matter of paramount significance given the persistent challenges municipal waste management poses for local authorities and enterprises [15]. Multiple studies have delved into the application of organic residues as adsorbents for chromium such as cocoa podhusk [16] or plantain peels [17]. For instance, one study [18] scrutinized the capability of tea waste in adsorbing Cr (VI). The analysis revealed the material had a peak adsorption capacity of 75.76 mg/g, coupled with commendable durability, retaining an adsorption efficacy surpassing 70% over five successive cycles. Another study [19] employed peanut shell waste to adsorb Cr (VI) from solutions, observing a zenith adsorption capacity of 2.36 mg/g.

Conversely, given their ample availability and affordability, corn by-products have attracted attention as prospective adsorbents for heavy metals. Research has been conducted on the efficacy of corn activated carbon in adsorbing Fe, Cu, and Pb from industrial wastewaters, reporting maximum removal efficiencies of 80.01%, 79.5%, and 79.89%, respectively [20]. Investigations into the use of corn cobs for Cd adsorption determined a peak adsorption capacity of 126.93 mg/g [21]. Studies have also shown corn cobs to be effective in extracting Cr (VI) from liquid solutions, noting a maximum adsorption value of 11.75 mg/g at pH 2 [22].

The enhancement of these natural adsorbents can be furthered by creating composites [23, 24]. A biocomposite utilizing Eriobotrya japonica seeds and sodium bentonite has been developed, exhibiting a robust adsorption capacity for copper, peaking at 63.56 mg/g [25]. Composite adsorbent from banana peel waste and silica have been prepared, targeting the removal of organic compounds. The adsorbent displayed adsorption capacities of 78.85 and 58.81 mg/g for methylene blue in synthetic wastewater and real samples, respectively [26]. Additionally, an adsorbent combining apple seeds and bentonite has been engineered for dye extraction, achieving maximum adsorption capacities of 1,439.9 mg/g for Congo red dye and 706.72 mg/g for malachite green dye [27].

In this context, repurposing organic wastes as adsorbents emerges as an avenue for either profitability or cost mitigation within the circular economy model. The goal of this study is to address the need for an effective, affordable, and sustainable method to eliminate chromium from wastewater, thereby safeguarding the environment and public health. This research delves into the application of a novel composite adsorbent formulated from corn residues for chromium removal. It thoroughly examines the kinetics and equilibrium of adsorption, employs the response surface methodology to optimize three variables of the adsorption process, and investigates the mechanisms involved in adsorption.

2. Materials and methods

2.1 Adsorbent preparation and characterization

The preparation of the adsorbent followed the methodology outlined elsewhere [25]. Initially, corn waste was left to air dry for a week. Subsequently, this dried residue was oven-dried at 50 °C until it reached a consistent weight. After the drying process, the waste was crushed using a pestle and mortar, and sieved to achieve a particle size under 0.25 mm. It was only after this stage that the corn waste was combined with bentonite in a 1:1 ratio. To ensure thorough mixing and a homogenous result, a small amount of distilled water was incorporated. The resulting mixture was then dried at 50 °C for a 24-hour period. Upon completion, it was taken out of the oven and allowed to cool to ambient temperature. This material underwent a subsequent round of grinding, blending with a small quantity of distilled water, drying, and sieving. The final adsorbent was then stored in airtight plastic bags in a dry setting until required.

The adsorbent characterization involved analyzing its chemical composition using energy-dispersive X-ray fluorescence spectrometry (ED-XRF). This process facilitated the identification of principal elements, employing a Shimadzu spectrometer, model EDX-800HS. Measurements were conducted on the ash sample under standard temperature conditions (22.1 °C) and at a relative humidity of 64%.

Further analysis to ascertain the functional groups present in the prepared adsorbent, both pre and post adsorption, was carried out using Fourier-transform infrared spectroscopy (FTIR). These FTIR analyses were performed utilizing a Frontier spectrometer, achieving a spectrum with a resolution of 4 cm^{-1}, and were conducted at a velocity of 0.2 cm/sec over two scans. The spectrum spanned from 4,000 to 400 cm^{-1}, using a universal ATR accessory with a diamond crystal/KRS-5 combination for single-bounce reflection.

2.2 Adsorption tests

For the adsorption experiments, a stock solution was created using potassium dichromate, formulated to contain a chromium concentration of 1000 mg/L. The experiments were executed in beakers, wherein the solution was agitated using a magnetic stirrer at ambient temperature. Upon reaching the predetermined adsorption duration, a 10 mL sample was taken from the mixture. This sample was then passed through filter paper and a funnel, separating the solid phase (the adsorbent) from the liquid phase (the treated solution). Chromium analysis was performed post-filtration. The concentration of hexavalent chromium remaining in the solution was ascertained utilizing a colorimetric method [28].

The efficiency of the adsorption (% Rem) was calculated using Equation (1), where Co represents the initial concentration (mg/L), and Ct denotes the concentration at time t (mg/L). Equation (2) was employed to determine the equilibrium adsorption capacity (Qe) in mg/g. In this equation, Ce signifies the equilibrium concentration of the adsorbate (mg/L), V stands for the total volume of the solution (L), and m is the mass of the adsorbent (g). All adsorption tests were conducted in duplicate.

$$\%R_{em} = \frac{C_0 - C_t}{C_0} \cdot 100 \quad (1)$$

$$Q_e = \frac{C_0 - C_e}{m} \cdot V \quad (2)$$

2.3 Adsorption kinetics

The initial adsorption experiments conducted were kinetic studies, designed to assess the rate of adsorption. For these tests, 500 mL of a mono-metallic solution with an initial chromium concentration of 100 mg/L was utilized. To this solution, 2.5 g of the prepared adsorbent was added. The mixture was then stirred continuously for a total duration of 36 hours. At predetermined intervals - 10 min, 20 min, 30 min, 1 h, 4 h, 12 h, 24 h, and 36 h - samples of the solution were collected for analysis. The pH was maintained at 6.20 ± 0.05 throughout the duration of the test. The kinetics of adsorption were analyzed using several models: pseudo-first order, pseudo-second order, Elovich, film diffusion, intraparticle diffusion, and pore diffusion models, as outlined in Table 1.

In this table, Qt represents the amount of adsorbate at equilibrium at time t, expressed in mg/g; t denotes the elapsed time in minutes; C the intercept and k2, ke, ki, kl, kp are the parameters of each model. C (mg/g) is the intercept of both the intraparticle diffusion model and

Table 1 Adsorption kinetics models

Kinetic model	Equation	Linear expression
Pseudo-first order	$\mathrm{Q_t = Q_e\,(1 - \exp\,(k_1 \cdot\ T))}$	$\log\,(Q_e - Q_t) = \log Q_e - \frac{k}{2.303} \cdot T$
Pseudo-second order	$Q_t = \frac{Q_e^2 \cdot k_2 \cdot T}{1 + Q_e \cdot k_2 \cdot T}$	$\frac{T}{Q_t} = \frac{1}{k_2 \cdot Q_e^2} + \frac{T}{Q_e}$
Elovich	$\mathrm{Q_t = \frac{1}{k_e}\ln\,(1 + Q_e \cdot k_e)}$	$\mathrm{Q_t = \frac{1}{k_e}\ln Q_e k_e + \frac{1}{k_e}\ln T}$
Intraparticle diffusion	$\mathrm{Q_t = k_i \cdot T^{1/2} + C}$	
Film diffusion	$\ln\left(1 - \frac{Q_e}{Q_t}\right) = -k_l \cdot T + C$	
Pore diffusion	$\log\log\left(\frac{C_0}{C_0 - Q_t \cdot m}\right) = \log\left(\frac{k_p \cdot m}{2.303V}\right) + \alpha \log_t$	

the film diffusion model. This parameter represents the boundary layer thickness. The parameters of each model represent the adsorption rate under the specific conditions for each model. k2 (g/mg.min) is the pseudo second order rate constant, ke (g/mg) is the Elovich constant, ki (mg/g.min$^{0.5}$) is the intraparticle diffusion rate constant, kl (min^{-1}) is the film diffusion rate constant, kp (L/g.min) is the pore diffusion rate constant.

2.4 Adsorption equilibrium

The second set of experiments investigated the adsorption equilibrium, aiming to assess how adsorption changes with different initial adsorbent dosages. In 1,000 mL beakers, 500 mL of a mono-metallic solution with an initial chromium concentration of 25 mg/L was placed. Each test utilized a varying amount of biochar (1 g, 2.5 g, 5 g, and 10 g). Each beaker, containing the solution and biochar, was set on a shaker for four hours. During these experiments, the initial pH was maintained at 6.50 ± 0.2, and the final pH was maintained at 6.90 ± 0.2. The adsorption equilibrium was examined using four isotherm models: Langmuir, Freundlich, Temkin, and Dubinin-Radushkevich (D-R) (see Table 2).

In Table 2, Qmax represents the maximum adsorption capacity in mg/g; and K_L, A_T, and e denote the model parameters. The Langmuir constant (K_L [L/mg]) represents the affinity between the adsorbent and the adsorbate, A_T (L/g) is the Temkin isotherm constant and it reflects the maximum binding energy, and e (kJ/mol) is the D-R isotherm parameter, related to the mean free energy of adsorption per mole of the adsorbate.

2.5 Optimization of the adsorption process

The third set of experiments focused on the optimization tests, for which the response surface methodology was applied utilizing a central composite rotatable design. This methodology is extensively adopted for tuning the parameters of adsorption operation conditions [29, 30]. The central composite rotatable design involved three independent variables at five levels (Table 3). The chosen levels for adsorption time, initial chromium concentration, and adsorbent dose are based on findings from previous studies [31–33].

The integration of three variables across five levels leads to a total of 20 experiments. Table 4 outlines the levels for each experiment.

2.6 Statistical analysis

The fitting of the experimental data to the adsorption kinetics and equilibrium models was analyzed using both linear and nonlinear regression. Nonlinear regression was performed using the values found in linear regression, employing the Solver tool from Excel with the GRG (Generalized Reduced Gradient) method. The best fit of the models was determined by comparing the determination coefficients (R^2).

Table 2 Adsorption Equilibrium Models

Kinetic model	Equation	Linear expression
Langmuir I	$Q_e = \frac{Q_{\max} \cdot K_L \cdot C_e}{1 + K_L \cdot C_e}$	$\frac{1}{Q_e} = \frac{1}{Q_{\max} \cdot K_L} \cdot \frac{1}{C_e} + \frac{1}{Q_{\max}}$
Langmuir II		$\frac{C_e}{Q_e} = \frac{1}{Q_{\max} \cdot K_L} + \frac{Ce}{Q_{\max}}$
Langmuir III		$\mathrm{Q_e} = \mathrm{Q_{max}} - \frac{1}{\mathrm{K_L}} \cdot \frac{\mathrm{Q_e}}{\mathrm{C_e}}$
Langmuir IV		$\frac{Q_e}{C_e} = KLQ_{\max} - KLQ_e$
Freundlich	$\mathrm{Q_e} = \mathrm{K_F} \cdot \mathrm{C_e^{1/n}}$	$\ln Q_e = \ln K_F + 1/n \cdot \ln C_e$
Temkin	$\mathrm{Q_e} = \mathrm{B_t} \cdot \ln(\mathrm{A_T} \cdot \mathrm{C_e})$	$Q_e = B_t \cdot \ln A_T + B_t \cdot \ln C_e$
D-R	$\mathrm{Q_e} = \mathrm{Q_{max}} \cdot \mathrm{e}^{-\beta\varepsilon^2}$	$\ln Q_e = \ln Q_{\max} - \beta\varepsilon^2$

Table 3 Variables and levels of the central composite rotatable design

Independent variables	Levels				
A = Contact time (hours)	0.5	1	1.5	2	4
B = Adsorbent dosage (g/L)	5	7.5	10	20	30
C = C_0 Cr (mg/L)	20	30	40	50	60

Table 4 Variables and levels of the central composite rotatable design

Run	Time (hours)	Adsorbent dosage (g/L)	C_0 Cr (mg/L)
1	-1	-1	-1
2	1	-1	-1
3	-1	1	-1
4	1	1	-1
5	-1	-1	1
6	1	-1	1
7	-1	1	1
8	1	1	1
9	-2	0	0
10	2	0	0
11	0	-2	0
12	0	2	0
13	0	0	-2
14	0	0	2
15	0	0	0
16	0	0	0
17	0	0	0
18	0	0	0
19	0	0	0
20	0	0	0

The experimental data from the optimization tests were fitted to a second-order polynomial equation (Equation 3).

$$y = \beta_0 + \sum_i \beta_j x_j + \sum_{i<j} \beta_{ij} x_i x_j + \sum_j \beta_{jj} x_j^2 + e \quad (3)$$

Where β represents each coefficient of the equation, x is each of the independent variables, and e is the error. To fit the experimental data to this equation, multiple regression analysis was used. Subsequently, analysis of variance (ANOVA) was performed to evaluate the statistical significance of the model. Statistical analyses were conducted using the Minitab software.

2.7 Reusability tests

The reusability tests were conducted with 500 mL of chromium solution at an initial concentration of 30 mg/L, using 7.5 g of adsorbent, and an adsorption time of 100 minutes. Using these parameters, the % Rem was evaluated over five successive cycles.

3. Results and discussions

3.1 Adsorbent characterization

Table 5 details the elements and oxides identified in the chemical characterization of the adsorbent. These results include ash, elemental, and oxide contents. The predominant elements are silicon (62%) and aluminum (29%). The major oxides present are aluminum oxide and silicon oxide, constituting 48% and 46%, respectively.

Table 5 Chemical Characterization of the Adsorbent

Parameter	Value (%)
Ashes	65.49
Elements	
Silicon	62.11
Aluminum	29.19
Calcium	3.90
Sulfur	2.11
Potassium	1.41
Iron	0.77
Phosphorus	0.52
Oxides	
Aluminum oxide	48.81
Silicon oxide	46.34
Potassium oxide	2.35
Calcium oxide	1.33
Iron oxide	0.50
Phosphorus oxide	0.49
Sulfur oxide	0.16

Figure 1 displays the infrared spectrum of the prepared adsorbent, highlighting the values of the identified peaks. Most of the absorption peaks are observed between the bands of 1,500 and 500 cm^{-1}.

The characterization of the adsorbent (Table 5) reveals that the predominant elements are silicon and aluminum, accompanied by minor quantities of calcium, sulfur, potassium, iron, and phosphorus. The oxides of these elements are also present, with aluminum oxide and silicon oxide being notably prevalent (48.81% and 46.34%, respectively). The silicon oxides might offer active sites interacting with chromium [34].

The peak at 3673.97 cm^{-1} could correspond to hydroxyl groups (OH-) linked to clay minerals. This absorption band spectrum is additionally associated with the contributions from cellulose, hemicellulose, and lignin within natural fibers [35, 36]. The peaks at 1,119.04 cm^{-1} and 1,026.41 cm^{-1} might be linked with the cellulose vibrations in organic material and the Si-O-Si bonds in the structure of silicon dioxides. The peak at 945.81 cm^{-1} may denote Al-OH bonds in aluminum oxide. The peak appearing at 855.87 cm^{-1} could suggest the presence of carbonate groups (CO_3^{2-}) in the specimen. The peaks within the 500-800 cm^{-1} range (834.68 cm^{-1}, 797.28 cm^{-1}, 778.01 cm^{-1}, and 694.74 cm^{-1}) are typically indicative of stretching vibrations of Si-O and Al-O bonds in the clay composition. Furthermore, the peaks at 531.61 cm^{-1}, 515.24 cm^{-1}, 443.11 cm^{-1}, and 415.35 cm^{-1} might also be linked with the Si-O and Al-O bonds [37].

FTIR analysis indicates the existence of functional groups commonly found in clay structures such as bentonite, corroborating the predominance of silicon and aluminum in the composition, as evidenced by the chemical analysis.

3.2 Adsorption kinetics

Figure 2 presents the experimental data on chromium removal percentage. It shows that the adsorption rate is initially rapid up until around minute 720, after which the percentage of chromium removal stabilizes.

Table 6 compiles the parameters for adsorption kinetics as determined by linear and nonlinear regression. This table also provides R^2 values to assess how well the regression models fit the experimental data. Notably, the highest R^2 value, 0.968, is achieved by the linear regression of the pseudo-first-order model. Conversely, the intraparticle diffusion model exhibits the best fit with an R^2 of 0.898.

Figure 2 illustrates that the adsorption pace is rapid up until the 720-minute mark (12 hours), after which the rate of removal levels off. This pattern implies that adsorption equilibrium is likely reached around this timeframe. Studies involving adsorbents comprised of organic substances and clay materials have documented stabilization of adsorption within the initial minutes or hours [25–27].

Referring to the coefficient of determination R^2 (Table 6), the pseudo-first order model seems to offer the most accurate depiction of the data based on linear regression, exhibiting an R^2 of 0.968. This model posits that the rate of adsorption is directly proportional to the concentration of the adsorbate remaining unadsorbed [38]. Herein, the parameter Qe denotes the maximal adsorption capacity and is quantified as 1.593 mg/g in the linear regression. Nonetheless, despite these findings, metal adsorption kinetics commonly align more closely with the pseudo-second order model [25–27]. This alignment indicates that the adsorption might be governed by a chemisorption process [39, 40], where the adsorbate forms stronger chemical bonds with the surface, and the adsorption rate depends on the adsorbate concentration and the available adsorption sites, which is consistent with the assumptions of the pseudo-second order model.

The variances observed among the different diffusion kinetics models (Table 6) can be attributed to the distinct diffusion mechanisms each model considers. The intraparticle diffusion model assumes the rate of adsorption is impeded by the diffusion of the adsorbate within the adsorbent particles. Here, the parameter ki represents the intraparticle diffusion rate constant, standing at 0.017 $mgg^{-1}min^{-0.5}$, hinting a moderately paced diffusion rate within the particles. The constant C, valued at 0.183, gauges the thickness of the boundary layer. An R^2 of 0.898 denotes a substantial fit to the data, indicating that intraparticle diffusion could be the primary limiting mechanism in this scenario.

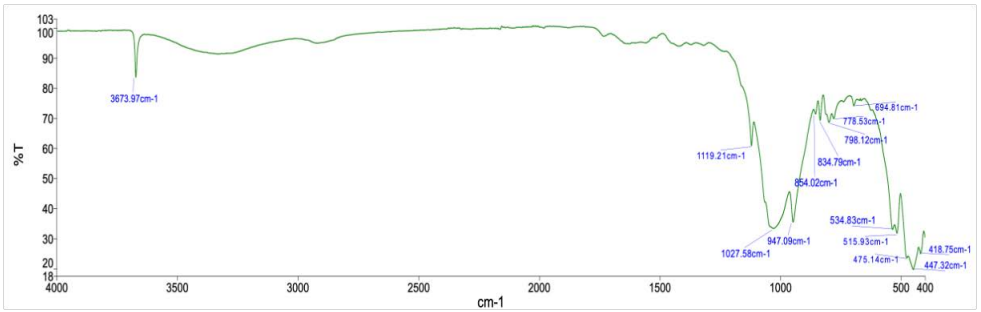

Figure 1 Block diagram of the system components

Table 6 Linear and nonlinear regression parameters for adsorption kinetics models

Model	Parameter	Linear regression	Nonlinear regression
Pseudo-first order	Q_e (mg/g)	1.593	10
	k_1 (min^{-1})	-0.002	-0.001
	R^2	0.968	0.902
Pseudo-second order	Q_e (mg/g)	0.867	10
	k_1 (g/mg*min)	0.013	479
	R^2	0.939	0.653
Elovich	Q_e (mg/g)	0.032	0.000
	k_1 (min^{-1})	7.225	50
	R^2	0.963	0.963
Intraparticle diffusion	k_i (mg*g^{-1}*$min^{-0.5}$)	0.017	–
	C	0.183	–
	R^2	0.898	–
Film diffusion	k_l (s^{-1})	0.003	–
	C	0.271	–
	R^2	0.847	–
Pore diffusion	k_p (g)	0.000	–
	α	0.339	–
	R^2	0.844	–

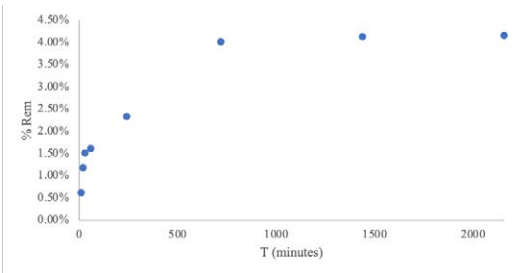

Figure 2 Chromium adsorption kinetics

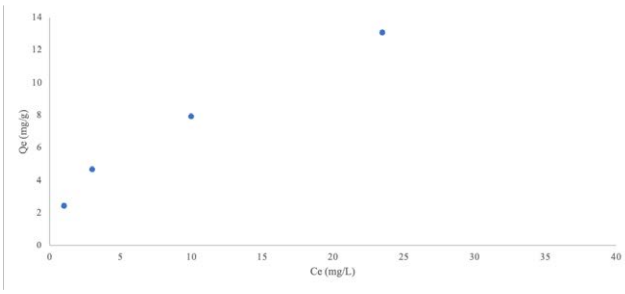

Figure 3 Chromium adsorption equilibrium curve

3.3 Adsorption equilibrium

Figure 3 displays the experimental data gathered from the adsorption equilibrium tests.

Table 7 details the parameter values of the various adsorption equilibrium models examined. These results indicate that the Freundlich model, with an R^2 of 0.997, exhibits the closest fit to the experimental data, followed by Langmuir I (R^2 = 0.988) and Temkin (R^2 = 0.942). Table 7 reveals that, within the Langmuir models, type I yielded the highest accuracy (R^2 = 0.988), manifesting a maximal adsorption capacity (Qmax) of 23.202 mg/g coupled with a Langmuir constant (K_L) of 0.037 L/mg. The fits for the other Langmuir forms were comparatively less precise. Meanwhile, the Freundlich model aligned most closely with the empirical data (R^2 = 0.997), showing K_F = 2.494 (mg/g)*(L/mg) and N at 1.918, signifying both a substantial adsorption capacity and relatively intense adsorption energy, respectively. The Temkin model also demonstrated a respectable congruence with the empirical data (R^2 = 0.942), and the parameters B_T and A_T were consistent across both linear and nonlinear regressions. Conversely, the D-R model recorded the lowest correlation with the empirical data.

Table 7 Linear and nonlinear regression parameters for adsorption equilibrium models

Model	Parameter	Linear regression	Nonlinear regression
Langmuir I	$Q_{\max}$ (mg/g)	23.202	7.896
	K_L (L/mg)	0.037	1
	R^2	0.988	0.797
Langmuir II	$Q_{\max}$ (mg/g)	46.948	–
	K_L (L/mg)	0.015	–
	R^2	0.652	–
Langmuir III	$Q_{\max}$ (mg/g)	28.49	–
	K_L (L/mg)	0.029	–
	R^2	0.710	–
Langmuir IV	$Q_{\max}$ (mg/g)	44.335	–
	K_L (L/mg)	0.017	–
	R^2	0.710	–
Freundlich	K_F (mg/g)*(L/mg)	2.494	2.460
	N	1.918	1.898
	R^2	0.997	0.997
Temkin	B_T (J/mol)	3.255	3.255
	A_T (L/g)	1.686	1.686
	R^2	0.942	0.942
D–R	β (mol^2/kJ^2)	0.938	1.885
	$Q_{\max}$ (mol/g)	11.282	11.380
	E (kJ/mol)	0.730	0.5156

In the field of metal adsorption systems, both Langmuir and Freundlich models are frequently employed to correlate with experimental data [39, 40]. These results underscore that the Freundlich model offers the most comprehensive explanation for chromium adsorption in this particular scenario, indicating that the adsorption process is intricate, potentially occurring at various sites each characterized by distinct adsorption energies. Throughout the duration of the experiment, pH values fluctuated between 6.50 ± 0.2 and 6.90 ± 0.2. This controlled pH range minimized the effects of pH variation on the adsorption process and the speciation of chromium in solution.

3.4 Optimization of the adsorption process

Table 8 presents the experimental conditions and outcomes alongside modeled results from the response surface experiments. The experimental percentage removal of chromium represents the mean of two replications for each run. Table 9 provides a detailed ANOVA for the response surface model. Equation 4 articulates the model deduced from the regression analysis, ANOVA, and significance of the coefficients.

$$\begin{aligned}\%\text{Rem Cr} = {} & -16.4 + 14.9\,\text{Time (h)} + 7.43\,\text{Dosage (g/L)} \\ & +1.09\,\text{CoCr(mg/L)} \\ & -3.12\,\text{Time(h)} * \text{Time(h)} \\ & -0.1008\,\text{Dosage(g/L)} * \text{Dosage(g/L)} \\ & -0.0183\,\text{CoCr(mg/L)} * \text{CoCr(mg/L)} \\ & -0.599\,\text{Time(h)*}\,\text{Dosage(g/L)} \\ & +0.219\,\text{Time(h)} * \text{CoCr(mg/L)} \\ & -0.0315\,\text{Dosage(g/L)} * \text{CoCr(mg/L)}\end{aligned} \quad (4)$$

Figure 4 depicts the response surface plots. The ANOVA demonstrates that the overall model holds significant value (p = 0.000), implying that at least one of the examined predictors effectively forecasts the response variable. Nonetheless, delving into the p-values of each individual coefficient reveals that not all predictors carry equal significance (Table 9).

The time coefficient is affirmative (14.9), suggesting an increment in the percentage of chromium removal concurrent with an increase in test duration. Despite this, its insignificance (p = 0.628) posits that test time might not be a dependable predictor for chromium elimination. Observing the response surface charts (Figure 4), it becomes evident that chromium removal rates escalate with time until reaching a plateau. Initially, the rapid phase of adsorption occurs as pollutants swiftly occupy accessible adsorption sites. Yet, as the procedure advances, fewer sites remain unoccupied, posing a challenge for any additional chromium ions to find available sites [20].

Regarding the initial coefficient of the concentration, its positivity (1.09) indicates an increase in the removal percentage of chromium parallel to the rise in initial chromium concentration. However, its statistical insignificance (p = 0.542) cannot be overlooked. The response surface plots (Figure 4c) indicate a diminishing efficiency in removal as the initial chromium concentration in the solution escalates. This phenomenon aligns with findings from other researchers, attributed to increased resistance in mass transfer between the liquid and solid phases as the contaminant concentration in the solution rises [41]. At lower chromium concentrations, more

Table 8 Adsorption test results

Run	Time (hours) (hours)	Adsorbent dosage (g/L)	C_0 Cr (mg/L)	% Rem Cr (experimental)	% Rem Cr (modeled)
1	1	7.5	30	73.60%	78.04%
2	2	7.5	30	78.04%	61.81%
3	1	20	30	99.55%	49.67%
4	2	20	30	99.91%	65.77%
5	1	7.5	50	68.84%	35.42%
6	2	7.5	50	78.63%	59.42%
7	1	20	50	87.55%	73.60%
8	2	20	50	90.29%	65.77%
9	0.5	10	40	49.67%	78.63%
10	4	10	40	68.01%	89.77%
11	1.5	5	40	35.42%	99.91%
12	1.5	30	40	89.77%	87.55%
13	1.5	10	20	61.98%	64.20%
14	1.5	10	60	45.89%	99.55%
15	1.5	10	40	61.81%	61.98%
16	1.5	10	40	65.77%	68.84%
17	1.5	10	40	59.42%	45.89%
18	1.5	10	40	65.77%	68.01%
19	1.5	10	40	64.20%	61.81%
20	1.5	10	40	61.81%	90.29%

Table 9 ANOVA for Optimization Model

Source	Sequential Sum of Squares	F Value	p value
Model	7315.3	6.21	0.000
Lineal	6405.8	2.40	0.088
Time (h)	121.7	0.24	0.628
Dosage (g/L)	5930.9	7.17	0.012
C_0 Cr (mg/L)	353.2	0.38	0.542
Square	774.5	2.09	0.123
Time (h)*Time (h)	89.2	1.92	0.176
Dosage (g/L)*Dosage (g/L)	542.0	4.96	0.034
C_0 Cr (mg/L)*C_0 Cr (mg/L)	143.2	1.07	0.308
Two-Factor Interaction	135.1	0.34	0.794
Time (h)*Dosage (g/L)	65.3	0.50	0.485
Time (h)*C_0 Cr (mg/L)	14.3	0.11	0.743
Dosage (g/L)*C_0 Cr (mg/L)	55.5	0.42	0.520
Error	3926.4		
Lack of fit	3827.9	194.17	0.000
Pure error	98.6		
Total	11241.8		
Standard Deviation	0.114	R^2	65.07%
PRESS	0.679	Adjusted R^2	54.59%
		Predictive R^2	39.56%

adsorption sites remain unengaged. However, with increasing chromium levels, the scarcity of available sites becomes pronounced, impacting the significance of this factor in adsorption efficiency. Therefore, at a lower initial concentration, such as 20 mg/L of chromium, adsorption sites are less saturated and face reduced competition compared to higher concentrations like 60 mg/L.

The dose coefficient, being positive (7.43), indicates an augmentation in chromium removal as the dose of the adsorbent surges, likely due to a greater number of adsorption sites [26]. Its significant p-value (p = 0.012) suggests that adsorbent dosage is a crucial predictor for chromium removal in this setting.

Finally, the optimal operating parameters were ascertained: a contact time of 103 minutes, an adsorbent dose of 29.71 g/l, and an initial chromium concentration of 31.13 mg/L.

3.5 Adsorption mechanism

Figure 5a illustrates the infrared spectrum following chromium adsorption, and Figure 5b compares the spectra before and after adsorption.

Analysis of the alterations in absorption frequencies within the FTIR spectrum, both pre- and post-adsorption (Figure 5b), sheds light on the types of chemical bonds engaged during adsorption. The peak located at 3,673.97 cm^{-1}

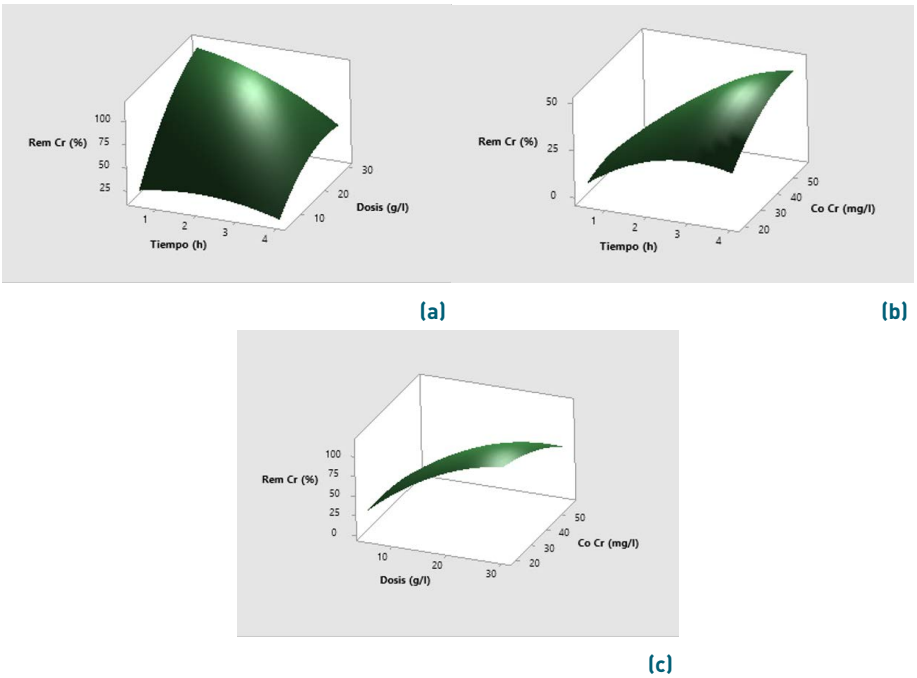

Figure 4 Response surface plots for chromium removal under the effect of (a) biochar dosage and time; (b) initial chromium concentration and time; and (c) biochar dosage and initial chromium concentration

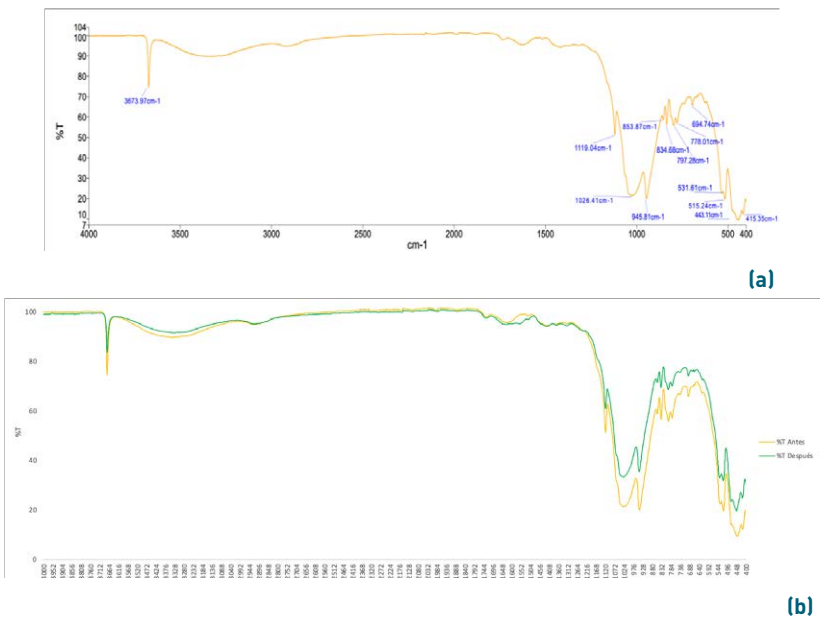

Figure 5 FTIR spectrum peaks of the adsorbent after adsorption (a) and comparison between before and after adsorption (b)

is likely linked to the vibrations of hydroxyl (OH) groups [37]. Observing the spectrum following adsorption, this peak remains unchanged, leading to the inference that the OH groups might not be actively participating in chromium adsorption, or any potential alterations are too subtle to detect. Frequencies noted at 945.81 cm^{-1} and 1,026.41 cm^{-1} are presumed to correlate with vibrations of Si-O and Al-O bonds, respectively. Post-adsorption, these peaks exhibit a slight shift to 947.09 cm^{-1} and 1,027.58 cm^{-1}, respectively. Such shifts may signal the engagement of chromium with the silicon and aluminum atoms, conceivably through either coordinated or ionic bonding. Notably, a new peak emerges at 475.14 cm^{-1} in the spectrum after adsorption, potentially signifying the formation of novel bonds or structural modifications of the material due to chromium adsorption. The

observed modifications in the FTIR spectra suggest that the adsorption process of chromium onto the adsorbent could involve interactions primarily with the silicon and aluminum constituents in the bentonite structure.

3.6 Reusability of the adsorbent

The outcomes derived from the reusability tests of the adsorbent are critical for assessing the real-world application potential of the bentonite and corn waste adsorbent in actual water treatment scenarios. Figure 6 displays the outcomes from the reusability tests of the adsorbent over five successive adsorption cycles.

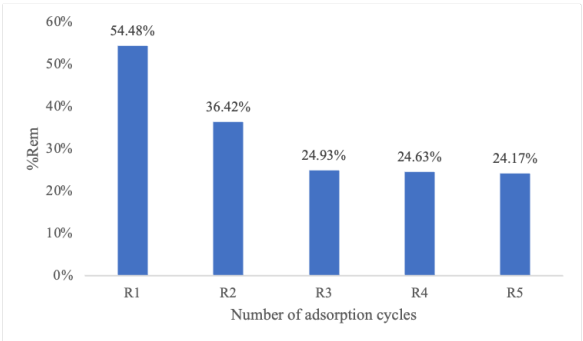

Figure 6 Adsorbent reusability in successive adsorption cycles

In the first adsorption cycle (R1) the adsorbent reached a %Rem of 54%. However, from the second cycle (R2), a decrease in efficiency can be observed, which dropped to 36%. From the third cycle (R3) onwards, the %Rem remained more or less constant, around 24-25%.

The %Rem observed in the inaugural adsorption cycle indicates that the adsorbent, upon its production and initial preparation for use, is highly effective in removing chromium. Nevertheless, the pronounced decline in efficiency observed from the second reuse cycle onward could stem from the saturation of adsorptive sites within the material. These sites, once filled with chromium during the initial cycle, reduce the capacity of the material to adsorb additional chromium in the subsequent cycles. During the later reusability cycles (R3 to R5), the %Rem appears to stabilize at approximately 24-25%. This trend might imply that, despite the initial drop in efficiency after the first few uses, the adsorbent retains a sustained, though reduced, capability to adsorb chromium.

4. Conclusions

In this research, a composite adsorbent was prepared for chromium removal. Characterization of the adsorbent demonstrates the effectiveness of the combination of bentonite and corn waste in creating an adsorbent with acceptable physical and chemical properties. The pseudo-first order model and the Elovich model presented significant fits to the data. The results of the diffusion models also suggest that intraparticle diffusion may be the limiting step in the adsorption process. The Freundlich model provided the best fit to the experimental data. In the response surface design, the most relevant factor for chromium removal is the adsorbent dosage. The optimum operating conditions are 103 minutes of contact, 29.71 g/L adsorbent and an initial chromium concentration of 31.13 mg/L.

Regarding the adsorption mechanisms, the findings demonstrate that chromium adsorption may be a multifaceted process involving chromium diffusion through the adsorbent matrix and subsequent interaction with adsorption sites on the surface and possibly at the edges of the bentonite layers. The FTIR spectrum after adsorption indicates changes in the Si-O and Al-O bonds, which suggest that chromium might be interacting with the silicon and aluminum atoms of the bentonite. Confirmation of the effectiveness of the prepared adsorbent supports opportunities for the development of low-cost and environmentally friendly solutions in the field of remediation of water contaminated with heavy metals.

Declaration of competing interest

We declare that we have no significant competing interests including financial or non-financial, professional, or personal interests interfering with the full and objective presentation of the work described in this manuscript.

Funding

The authors received no financial support for the research, authorship, and/or publication of this article.

Author contributions

M. E. Herrera-Gavidia: Conceived and designed the study, conducted the research, provided study materials and resources, administered the project, and performed the formal analysis. D. Carbonel: Developed the methodology, performed the formal analysis, and wrote the initial draft of the paper. H. Chirinos-Collantes: Oversaw and led the research, developed the methodology, and performed the formal analysis.

Data available statement

The datasets generated during and/or analyzed during the current study are available from the corresponding author on reasonable request.

References

[1] R. T. Kapoor, M. F. Bani-Mfarrej, P. Alam, J. Rinklebe, and P. Ahmad, "Accumulation of chromium in plants and its repercussion in animals and humans," *Environmental Pollution*, vol. 301, May 2022. [Online]. Available: https://doi.org/10.1016/j.envpol.2022.119044

[2] A. Bakshi and A. K. Panigrahi, "A comprehensive review on chromium induced alterations in fresh water fishes," *Toxicology Reports*, vol. 5, 2018. [Online]. Available: https://doi.org/10.1016/j.toxrep.2018.03.007

[3] G. Lian, B. Wang, X. Lee, L. Li, T. Liu, and W. Lyu, "Enhanced removal of hexavalent chromium by engineered biochar composite fabricated from phosphogypsum and distillers grains," *Science of The Total Environment*, vol. 697, Dec 2019. [Online]. Available: https://doi.org/10.1016/j.scitotenv.2019.134119

[4] Nakkeeran, C. Patra, T. Shahnaz, S. Rangabhashiyam, and N. Selvaraju, "Continuous biosorption assessment for the removal of hexavalent chromium from aqueous solutions using strychnos *nux vomica* fruit shell," *Bioresource Technology Reports*, vol. 3, Sep 2018. [Online]. Available: https://doi.org/10.1016/j.biteb.2018.09.001

[5] S. Prasad, K. K. Yadav, S. Kumar, N. Gupta, M. M. S. Cabral-Pinto, S. Rezania *et al.*, "Chromium contamination and effect on environmental health and its remediation: A sustainable approaches," *Journal of Environmental Management*, vol. 285, May 2021. [Online]. Available: https://doi.org/10.1016/j.jenvman.2021.112174

[6] M. Nur-E-Alam, M. A. S. Mia, F. Ahmad, and M. M. Rahman, "An overview of chromium removal techniques from tannery effluent," *Appl Water Sci*, vol. 10, no. 9, Sep 2020. [Online]. Available: https://doi.org/10.1007/s13201-020-01286-0

[7] H. M. Córdova-Bravoa, R. Vargas-Parker, M. F. Cesare-Coral, L. F. del Pino, and L. Visitació-Figueroa, "Tratamiento de las aguas residuales del proceso de curtido tradicional y alternativo que utiliza acomplejantes de cromo," *Revista de la Sociedad Química del Perú*, vol. 80, no. 3, 2014. [Online]. Available: https://www.redalyc.org/articulo.oa?id=371937639005

[8] P. M. Condori-Ramos and M. A. Pumacayo-Gutiérrez, "Evaluación de la remediación de aguas contaminadas con cromo empleando una columna de lecho fijo con biomasa de cáscara de papa 'solanum tuberosum' arequipa 2019," 2019, accessed: Nov. 23, 2023. [Online]. Available: https://repositorio.ucsm.edu.pe/handle/20.500.12920/9527

[9] M. A. Irshad, S. Sattar, R. Nawaz, S. A. Al-Hussain, M. Rizwan *et al.*, "Enhancing chromium removal and recovery from industrial wastewater using sustainable and efficient nanomaterial: A review," *Ecotoxicol Environ Saf*, vol. 263, Sep 2023. [Online]. Available: https://doi.org/10.1016/j.ecoenv.2023.115231

[10] S. S. Kerur, S. Bandekar, M. S. Hanagadakar, S. S. Nandi, G. M. Ratnamala, and P. G. Hegde, "Removal of hexavalent chromium-industry treated water and wastewater: A review," *Materials Today Proceedings*, vol. 42, 2021. [Online]. Available: https://doi.org/10.1016/j.matpr.2020.12.492

[11] K. GracePavithra, V. Jaikumar, P. S. Kumar, and P. SundarRajan, "A review on cleaner strategies for chromium industrial wastewater: Present research and future perspective," *Journal of Cleaner Production*, vol. 228, Aug. 2019. [Online]. Available: https://doi.org/10.1016/j.jclepro.2019.04.117

[12] R. Chakraborty, A. Asthana, A. K. Singh, B. Jain, and A. B. H. Susan, "Adsorption of heavy metal ions by various low-cost adsorbents: a review," *International Journal of Environmental Analytical Chemistry*, vol. 102, no. 2, Jan. 2022. [Online]. Available: https://doi.org/10.1080/03067319.2020.1722811

[13] E. A. Ashour and M. A. Tony, "Eco-friendly removal of hexavalent chromium from aqueous solution using natural clay mineral: activation and modification effects," *SN Appl Sci*, vol. 2, no. 12, Dec 2020. [Online]. Available: https://doi.org/10.1007/s42452-020-03873-x

[14] A. A. Jock, I. O. Oboh, U. E. Inyang, L. P. Ganchok, and O. Adeku, "Chromium and nickel metal ions removal from contaminated water using nigerian bentonite clay," *Water Pract Technol*, vol. 16, no. 3, Jul 2021. [Online]. Available: https://doi.org/10.2166/wpt.2021.031

[15] V. E. Olivo, P. D. M. Prietto, and E. P. Korf, "Review of guidelines for sustainable municipal waste management: best practices in brazil," *Proceedings of the Institution of Civil Engineers - Waste and Resource Management*, vol. 175, no. 2, May 2022. [Online]. Available: https://doi.org/10.1680/jwarm.21.00017

[16] L. L. Pérez-Antolinez, I. C. Pa-Astudillo, A. P. Sandoval-Aldana, and G. C. Peñaloza-Atuesta, "Uso de cáscara de cacao (theobroma cacao) para la remocion de cromo en solución acuosa," *Revista EIA*, vol. 17, no. 34, Nov. 2020. [Online]. Available: https://doi.org/10.24050/reia.v17i34.1393

[17] C. Tejada-Tovar, A. Villabona-Ortíz, and R. Ortega-Toro, "Determination of kinetic parameters in the biosorption of chromium (vi) in aqueous solution," *Ing Cienc*, vol. 16, no. 31, Jun. 2020. [Online]. Available: https://doi.org/10.17230/ingciencia.16.31.6

[18] S. Fan, Y. Wang, Y. Li, J. Tang, Z. Wang, J. Tang *et al.*, "Facile synthesis of tea waste/fe_3o_4 nanoparticle composite for hexavalent chromium removal from aqueous solution," *RSC Advances*, no. 13, 2017. [Online]. Available: https://doi.org/10.1039/C6RA27781K

[19] J. Bayuo, M. A. Abukari, and K. B. Pelig-Ba, "Optimization using central composite design (ccd) of response surface methodology (rsm) for biosorption of hexavalent chromium from aqueous media," *Applied Water Science*, vol. 10, no. 135, 2020. [Online]. Available: https://doi.org/10.1007/s13201-020-01213-3

[20] I. Christica and R. Julia, "Activated carbon utilization from corn cob (zea mays) as a heavy metal adsorbent in industrial waste," *Asian Journal of Pharmaceutical Research and Development*, vol. 6, no. 5, Oct 2018. [Online]. Available: https://doi.org/10.22270/ajprd.v6i5.411

[21] A. Villabona-Ortíz, C. Tejada-Tovar, and A. D. Gonzalez-Delgado, "Adsorption of cd^{2+} ions from aqueous solution using biomasses of *Theobroma cacao*, *Zea mays*, *Manihot esculenta*, *Dioscorea rotundata* and *Elaeis guineensis*," *Applied Sciences*, vol. 11, no. 6, Mar. 2021. [Online]. Available: https://doi.org/10.3390/app11062657

[22] I. Polowczyk, T. Kozlecki, J. Ulatowska, and A. Bastrzyk, "Solid waste materials for arsenic and chromium removal," in *Innovative Materials and Methods for Water Treatment*. Leiden: CRC Press, 2016, pp. 217–256.

[23] R. Foroutan, R. Mohammadi, A. S. Adeleye, S. Farjadfard, Z. Esvandi, H. Arfaeinia *et al.*, "Efficient arsenic(v) removal from contaminated water using natural clay and clay composite adsorbents," *Environmental Science and Pollution Research*, vol. 26, Oct. 2019. [Online]. Available: https://doi.org/10.1007/s11356-019-06070-5

[24] S. K. M. T. Hossain, P. K. Shaha, U. Rayhan, A. Islam, T. R. Choudhury *et al.*, "Functionalized layered double hydroxides composite bio-adsorbent for efficient copper(ii) ion encapsulation from wastewater," *J Environ Manage*, vol. 300, Dec. 2021. [Online]. Available: https://doi.org/10.1016/j.jenvman.2021.113782

[25] M. Mushtaq, H. N. Bhatti, M. Iqbal, and S. Noreen, "*Eriobotrya japonica* seed biocomposite efficiency for copper adsorption: Isotherms, kinetics, thermodynamic and desorption studies," *Journal of Environmental Management*, vol. 176, Jul. 2016. [Online]. Available: https://doi.org/10.1016/j.jenvman.2016.03.013

[26] S. M. Ali, "Fabrication of a nanocomposite from an agricultural waste and its application as a biosorbent for organic pollutants," *International Journal of Environmental Science and Technology*, vol. 15, Jul. 2018. [Online]. Available: https://doi.org/10.1007/s13762-017-1477-x

[27] M. A. Adebayo, J. I. Adebomi, T. O. Abe, and F. I. Areo, "Removal of aqueous congo red and malachite green using

ackee apple seed–bentonite composite," *Colloid and Interface Science Communications*, vol. 38, Sep. 2020. [Online]. Available: https://doi.org/10.1016/j.colcom.2020.100311

[28] American Public Health Association (APHA) and American Water Works Association (AWWA) and Water Environment Federation (WEF), *Standard Methods for the Examination of Water and Wastewater*, 24th ed. American Waterworks Association, 2022.

[29] A. A. Oyekanmi, A. Ahmad, K. Hossain, and M. Rafatullah, "Adsorption of rhodamine b dye from aqueous solution onto acid treated banana peel: Response surface methodology, kinetics and isotherm studies," *PLoS One*, vol. 14, no. 5, May 2019. [Online]. Available: https://doi.org/10.1371/journal.pone.0216878

[30] Z. Anfar, H. A. Ahsaine, M. Zbair, A. Amedlous, A. A. El-Fakir, A. Jada *et al.*, "Recent trends on numerical investigations of response surface methodology for pollutants adsorption onto activated carbon materials: A review," *Critical Reviews in Environmental Science and Technology*, vol. 50, no. 10, Jul. 2020. [Online]. Available: https://doi.org/10.1080/10643389.2019.1642835

[31] R. Foroutan, S. J. Peighambardoust, R. Mohammadi, M. Omidvar, G. A. Sorial, and B. Ramavandi, "Influence of chitosan and magnetic iron nanoparticles on chromium adsorption behavior of natural clay: Adaptive neuro-fuzzy inference modeling," *International Journal of Biological Macromolecules*, vol. 151, May 2020. [Online]. Available: https://doi.org/10.1016/j.ijbiomac.2020.02.202

[32] J. Geng, Y. Yin, Q. Liang, Z. Zhu, and H. Luo, "Polyethyleneimine cross-linked graphene oxide for removing hazardous hexavalent chromium: Adsorption performance and mechanism," *Chemical Engineering Journal*, vol. 361, Apr. 2019. [Online]. Available: https://doi.org/10.1016/j.cej.2018.10.141

[33] M. E. González-López, C. M. Laureano-Anzaldo, A. A. Pérez-Fonseca, M. Arellano, and J. R. Robledo-Ortíz, "Chemically modified polysaccharides for hexavalent chromium adsorption," *Separation & Purification Reviews*, vol. 50, no. 4, Jun. 2020. [Online]. Available: https://doi.org/10.1080/15422119.2020.1783311

[34] B. O. Otunola and O. O. Ololade, "A review on the application of clay minerals as heavy metal adsorbents for remediation purposes," *Environmental Technology & Innovation*, vol. 18, May 2020. [Online]. Available: https://doi.org/10.1016/j.eti.2020.100692

[35] M. W. Amer, J. S. Aljariri-Alhesan, S. Ibrahim, G. Qussay, M. Marshall, and O. S. Al-Ayed, "Potential use of corn leaf waste for biofuel production in jordan (physio-chemical study)," *Energy*, vol. 214, Jan. 2021. [Online]. Available: https://doi.org/10.1016/j.energy.2020.118863

[36] J. Ponce, J. G. D. Silva-Andrade, L. N. dos Santos, M. Keller-Bulla, B. C. Bolanho-Barros, S. L. Favaro *et al.*, "Alkali pretreated sugarcane bagasse, rice husk and corn husk wastes as lignocellulosic biosorbents for dyes," *Carbohydrate Polymer Technologies and Applications*, vol. 2, Dec. 2021. [Online]. Available: https://doi.org/10.1016/j.carpta.2021.100061

[37] G. Henderson, D. Neuville, and R. Downs, "Spectroscopic methods in mineralogy and material sciences," in *Reviews in Mineralogy & Geochemistry*. Berlin, Boston: De Gruyter, 2014. [Online]. Available: https://doi.org/10.1515/9781614517863

[38] E. D. Revellame, D. L. Fortela, W. Sharp, R. Hernandez, and M. E. Zappi, "Adsorption kinetic modeling using pseudo-first order and pseudo-second order rate laws: A review," *Cleaner Engineering and Technology*, vol. 1, Dec. 2020. [Online]. Available: https://doi.org/10.1016/j.clet.2020.100032

[39] E. H. Gürkan, B. Ílyas, and Y. Tibet, "Adsorption performance of heavy metal ions from aqueous solutions by a waste biomass based hydrogel: comparison of isotherm and kinetic models," *International Journal of Environmental Analytical Chemistry*, vol. 103, no. 6, May 2023. [Online]. Available: https://doi.org/10.1080/03067319.2021.1873314

[40] F. Xiao, J. Cheng, W. Cao, C. Yang, J. Chen, and Z. Luo, "Removal of heavy metals from aqueous solution using chitosan-combined magnetic biochars," *Journal of Colloid and Interface Science*, vol. 540, Mar. 2019. [Online]. Available: https://doi.org/10.1016/j.jcis.2019.01.068

[41] X. Chen, M. F. Hossain, C. Huan, J. Lu, Y. F. Tsang, M. S. Islam *et al.*, "Isotherm models for adsorption of heavy metals from water - a review," *Chemosphere*, vol. 307, Nov. 2022. [Online]. Available: https://doi.org/10.1016/j.chemosphere.2022.135545